Journal of Materials Chemistry

Cite this: *J. Mater. Chem.*, 2012, **22**, 19236

www.rsc.org/materials

PAPER

Incorporating a stable fluorenone unit into D–A–π–A organic dyes for dye-sensitized solar cells

Chuanjiang Qin, Ashraful Islam and Liyuan Han*

Received 16th May 2012, Accepted 4th August 2012
DOI: 10.1039/c2jm33105e

Two new organic dyes based on a donor–acceptor–π–bridge–acceptor/anchor (D–A–π–A) configuration, **HIQF1** and **HIQF2**, were synthesized, characterized, and successfully employed in dye-sensitized solar cells. The incorporation of the weakly electron-withdrawing fluorenone group as an additional acceptor enhanced the dyes' properties for solar energy conversion in several ways. First, the absorption spectra of the dyes were broadened, covering a large range of sunlight. Second, the absorption spectra observed upon dye adsorption on TiO_2 were only slightly blue-shifted as compared to the spectra of the dyes in solution. Third, the orbital energy levels and electron distributions of the D–A–π–A backbone were ideal for highly efficient electron transport and injection. The incorporation of long electron-donating alkoxy groups in the donor unit of **HIQF1** further increased the dye's short-circuit photocurrent density (J_{sc}), open-circuit voltage (V_{oc}), and overall conversion efficiency (η), but had little negative effect on the fill factor (FF). Solar cells sensitized with **HIQF1** showed excellent current–voltage characteristics; the J_{sc}, V_{oc}, and FF values were 12.26 mA cm^{-2}, 0.70 V, and 0.73, corresponding to a η value of 6.26%.

Introduction

Metal-free organic dyes have sparked a flurry of research activity in the scientific community owing to their potential application as highly efficient photosensitizers in dye-sensitized solar cells (DSCs).[1] Metal-free organic dyes, which are normally constructed with a donor–π–bridge–acceptor (D–π–A) configuration, hold great promise owing to their high molar extinction coefficients, facile structure modification, and no concern of the rare metal resource.[2] However, the overall conversion efficiencies of DSCs based on metal-free organic dyes are lower than those of DSCs based on ruthenium dyes, owing to the metal-free organic dyes' narrow coverage of the solar spectrum. Thus, there is growing interest in developing new sensitizers with broader absorption for DSCs applications. Recent research endeavours toward this goal have involved the use of additional acceptor chromophores between the donor and the π-bridge of the dye molecule, leading to a D–A–π–A architecture, which facilitates intramolecular charge transfer and shifts the bandgap energy to permit harvesting of sunlight from a larger range of wavelengths. For example, benzothiadiazole, quinoxaline, and benzotriazole have been incorporated in D–A–π–A configurations as additional acceptors, and the resulting molecules exhibit good cell performance and stability.[3] Such favourable results encourage us to continually explore new functional groups as additional acceptors for highly efficient and low-cost DSCs.

Fluorene derivatives have been widely applied in polymer solar cells, polymer light-emitting diodes, and multiphoton-absorbing materials owing to their unique electrochemical and optical properties and their excellent hole-transporting abilities.[4] Recently, Zhu *et al.* introduced fluorene into D–π–A organic dyes as a conjunction bridge and used the resulting dyes in TiO_2 DSCs.[5] However, the conversion efficiency of even the best DSCs constructed from these dyes is low (4.26%), owing to the narrow absorption spectrum of the dye that results from its absorption on TiO_2. Incorporating electron-withdrawing groups, such as ketones, at the C-9 position of fluorene stabilizes its LUMO, thus remarkably enhancing the electrophilicity of the molecule. Thus, fluorenone derivatives have been used as photosensitizers for carbazole-containing conductive polymers.[6] At the same time, fluorenone derivatives modified with electron-donating groups demonstrate a broadened absorption range due to charge transfer from donor units to the carbonyl group.[7] It is also worth mentioning that fluorenone should also more benefit for stability of DSCs due to its stable chemical property compared to fluorene that had been proved in the yield of above mentioned optical materials. Fluorenone is also attractive because it is commercially available and inexpensive. For these reasons, we sought to exploit the properties of fluorenone and D–A–π–A architectures to develop a new sensitizer for DSCs. In this paper, we report for the first time two novel fluorenone-based sensitizer dyes, **HIQF1** and **HIQF2** (Scheme 1), in which fluorenone is used as an additional acceptor, substituted triphenylamines are used as

Photovoltaic Materials Unit and NIMS Saint-Gobain Center of Excellence for Advanced Materials, National Institute for Materials Science, Sengen 1-2-1, Tsukuba, Ibaraki 305-0047, Japan. E-mail: Han.Liyuan@nims.go.jp; Fax: +81 29-859-2304; Tel: +81 29-859-2305

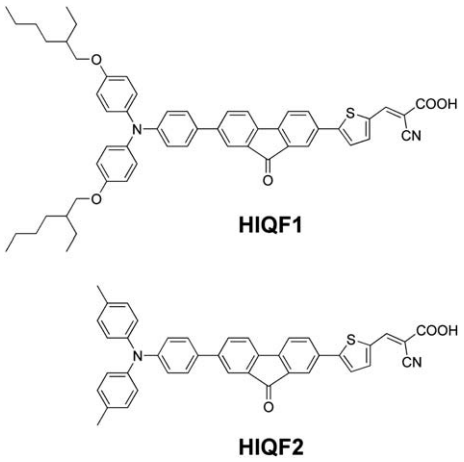

Scheme 1 Chemical structures of **HIQF1** and **HIQF2**.

donors, thiophene is a π-spacer, and 2-cyano-2-propenoic acid is an acceptor/anchor. We studied the influence of long alkyl chains on photovoltaic performance using controlled intensity-modulated photovoltage spectroscopy and achieved excellent current–voltage characteristics (J_{sc}, V_{oc}, and FF) of 12.26 mA cm^{-2}, 0.70 V, and 0.73, corresponding to an high overall conversion efficiency (η) of 6.26% for **HIQF1**.

Results and discussion

Synthesis and characterization

Scheme 2 shows the synthetic protocol for the new organic dyes, **HIQF1** and **HIQF2**. Each of the two dye precursors was easily prepared *via* two sequential asymmetrical Suzuki coupling reactions of 2,7-dibromofluorenone, first with a substituted triphenylamino borate and then with 5-formylthiophen-2-boronic acid. The resulting monoaldehyde-substituted precursors were subjected to Knoevenagel condensations with cyanoacetic acid to afford **HIQF1** and **HIQF2**. Purification of the mixtures by silica chromatography furnished **HIQF1** and **HIQF2** as air-stable black powders with high purity. The dyes were fully characterized by ^{1}H and ^{13}C NMR spectroscopy as well as mass spectrometry. The obtained dyes were deep red solids and were soluble in common organic solvents, such as chloroform, dimethylformamide (DMF), and acetonitrile.

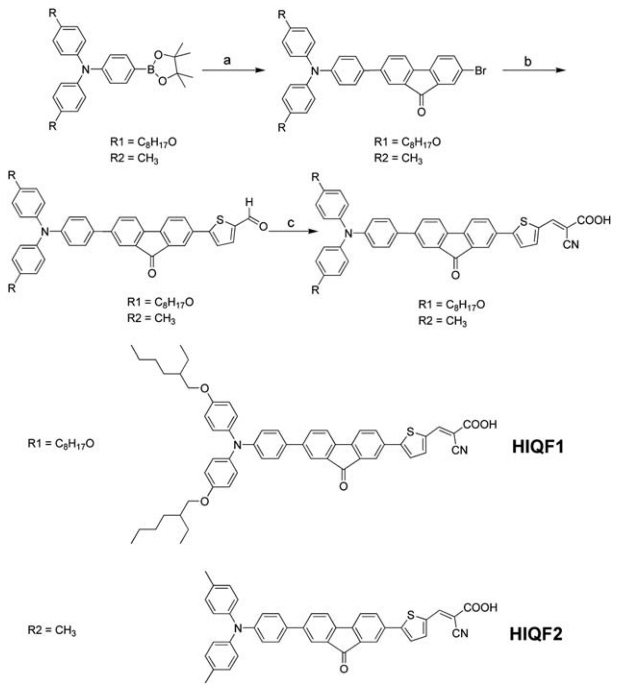

Scheme 2 Synthetic routes of **HIQF1** and **HIQF2**: (a) 2,7-dibromofluorenone, toluene, 2 M K_2CO_3, $Pd(PPh_3)_4$, reflux; (b) 5-formylthiophen-2-boronic acid, toluene, methanol, K_2CO_3, $Pd(dppf)Cl_2$, microwave, reflux; (c) $CNCH_2COOH$, piperidine, chloroform, reflux.

Photophysical characterization

Fig. 1 depicts the ultraviolet-visible (UV-vis) spectra of **HIQF1** and **HIQF2** measured in DMF. All spectroscopic data for **HIQF1** and **HIQF2** are listed in Table 1. The intense absorption peaks at 396 nm ($\varepsilon = 5.32 \times 10^4$ M^{-1} cm^{-1}) for **HIQF1** and 393 nm ($\varepsilon = 4.98 \times 10^4$ M^{-1} cm^{-1}) for **HIQF2** were attributed to the π–π* transitions of the conjugated aromatic moieties. The weak and low-energy bands observed at around 500 nm for **HIQF1** and **HIQF2** corresponded to intramolecular charge transfer absorption. Estrada *et al.* also reported similar weak absorption features with absorption band at around 440 nm for fluorenone-based donor–acceptor–donor type molecules without cyano unit.[8]

Both **HIQF1** and **HIQF2** with donor–π–bridge–acceptor configuration showed a broad and red shifted absorption band due to introduction of the thiophene group, and the strongly electron-withdrawing character of the cyano unit, which enhanced interaction between the donor and acceptor. When adsorbed on a transparent TiO_2 electrode (4 μm thickness), both dyes showed similar absorption spectra, and the absorption peaks were slightly blue-shifted compared with the corresponding peaks in the solution absorption spectra, due to deprotonation of the anchoring group and differences in the polarity of the media (Fig. 2).[9] Both in solution and on TiO_2, the absorption peaks of **HIQF1** were located at longer wavelengths ($\lambda_{abs.\ in\ DMF} = 396$, 482 nm; $\lambda_{abs.\ on\ TiO2} = 392$ nm) than those of **HIQF2** ($\lambda_{abs.\ in\ DMF} = 393$, 477 nm; $\lambda_{abs.\ on\ TiO2} = 385$ nm). The introduction of the electron-donating alkoxy group into the triphenylamino moiety of the **HIQF1** donor should have

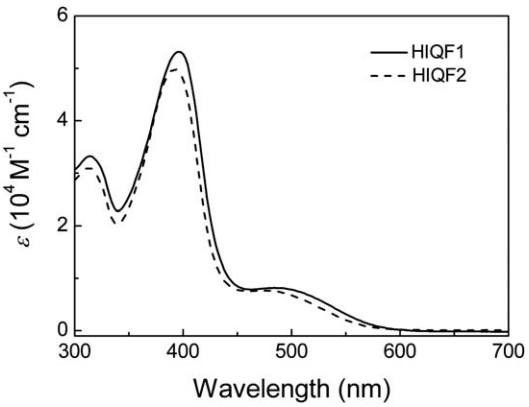

Fig. 1 UV-vis absorption spectra of **HIQF1** and **HIQF2** in DMF.

Table 1 Absorption and electrochemical properties of **HIQF1** and **HIQF2**

Dye	Absorption[a] [nm] (ε^b [10^3 M^{-1} cm^{-1}])	λ_{max} on TiO_2 [nm][c]	E_{0-0} [V][d]	E_{ox} [V][e]	E_{ox}^* [V][f]
HIQF1	396 (53.2), 484 (8.2)	392	2.10	1.02	−1.08
HIQF2	393 (49.8), 477 (7.7)	385	2.16	1.15	−1.01

[a] Absorption peaks of dyes in DMF. [b] Molar absorption coefficient determined from the absorbance for a molar concentration (2×10^{-6} M) of the dyes with a path length of 1 cm at corresponding wavelength. [c] Absorption maximum on TiO_2. [d] Optical bandgap $E_{0-0} = hc/\lambda_{onset}^{abs} = 1238.83/\lambda_{onset}^{abs}$. [e] $E_{ox} = |E_{pc} + E_{pa}|/2$ with the cathodic and anodic peak potentials E_{pa}, E_{pc} from the oxidation wave. [f] $E_{ox}^* = E_{ox} - E_{0-0}$.

increased the donor–acceptor character of the dye, thus explaining the observed red-shift in the absorption spectra of **HIQF1** compared with **HIQF2**. These results indicate that introducing fluorenone into the D–A–π–A architecture can effectively narrow the bandgap and thus permit the harvesting of more sunlight, both for the dye in solution and adsorbed on TiO_2.

Electrochemical characterization

The electrochemical properties of **HIQF1** and **HIQF2** were measured by cyclic voltammetry in a typical three-electrode electrochemical cell, with the dye-sensitized TiO_2 films serving as the working electrodes and 0.1 M tetra-*n*-butylammonium hexafluorophosphate as the supporting electrolyte (Table 1). The reference electrode was Ag/AgCl calibrated with Fc^+/Fc as an internal reference. **HIQF1** exhibited a reversible oxidative wave with a oxidation potential, E_{ox}, at 1.02 V (*vs.* NHE); whereas a reversible oxidative wave with a E_{ox} at 1.15 V was observed for **HIQF2** (Fig. 3). These values were low enough for efficient regeneration of the oxidized dyes *via* electron donation from iodide (~0.4 V *vs.* NHE).[10] **HIQF1**, which has an alkoxy-substituted triphenylamino donor unit, had an oxidation potential *ca.* 100 mV more negative than that of **HIQF2**, which has a methyl-substituted triphenylamino donor unit. This result indicates that the introduction of electron-donating alkoxy groups to the triphenylamino moiety caused a negative shift in the anodic E_{ox}. The excited-state oxidation potential values, E_{ox}^*, of the two dyes were calculated from their oxidation potentials (E_{ox}) and the optical energy gaps, E_{0-0}, determined from the onset value of the absorption spectra on transparent TiO_2 films.[11] The E_{0-0} values for **HIQF1** and **HIQF2** were 2.10 and 2.16 eV, respectively. The calculated E_{ox}^* values for **HIQF1** and **HIQF2** were −1.08 and −1.01 V (*vs.* NHE), respectively, and were much more negative than the conduction-band level of TiO_2 (approximately −0.5 V *vs.* NHE).[12] These results indicate a sufficient driving force for electron injection from the excited state of the sensitizer dyes to the TiO_2 conduction band.

Theoretical approach

It is important for an efficient sensitizer dye to possess a well-delocalized π-framework and directional electron distributions. To gain better insight into the electron distributions and molecular geometries of the dyes, we performed time-dependent density functional theory calculations, and the optimized molecular structures and frontier molecular orbital profiles are shown in Fig. 4. Molecular-orbital calculations showed that the HOMO was mainly delocalized on the triphenylamino unit for both **HIQF1** and **HIQF2**. These results suggest that delocalization of the HOMO on the donor moiety may facilitate reduction of the oxidized dye by reaction with I^-, making the dye suitable for highly efficient solar cells. The LUMOs of **HIQF1** and **HIQF2** were located predominantly on the cyanoacetic acid units and extended to the fluorenone moieties. Such electron distributions facilitate electron injection from the photoexcited sensitizer dye to TiO_2. Thus, HOMO–LUMO excitation would move the photoexcited electrons on the π-framework from the donor unit to the cyanoacrylic acid moiety *via* the additional acceptor-fluorenone group, which also is beneficial for efficient charge separation and electron injection. Moreover, since it is more weakly electrophilic than the cyano group, the electron-withdrawing ketone unit of the fluorenone does not limit electron injection. In our previous study, 4*H*-cyclopenta[2,1-*b*:3,4-*b*']

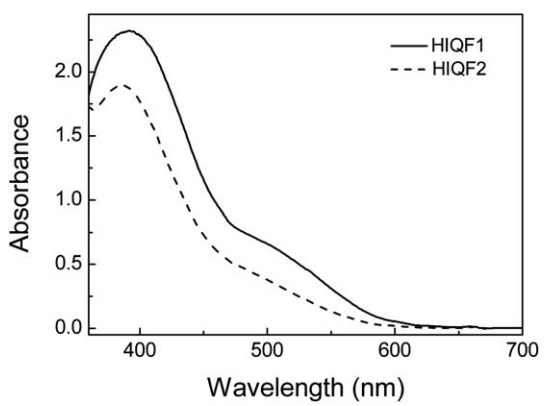

Fig. 2 UV-vis absorption spectra of **HIQF1** and **HIQF2** on TiO_2 nanoparticles.

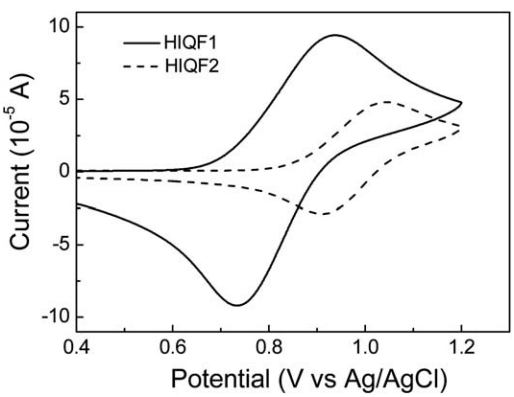

Fig. 3 Cyclic voltammetry of **HIQF1** and **HIQF2** adsorbed on TiO_2 film (4 μm thickness) deposited on TCO glass.

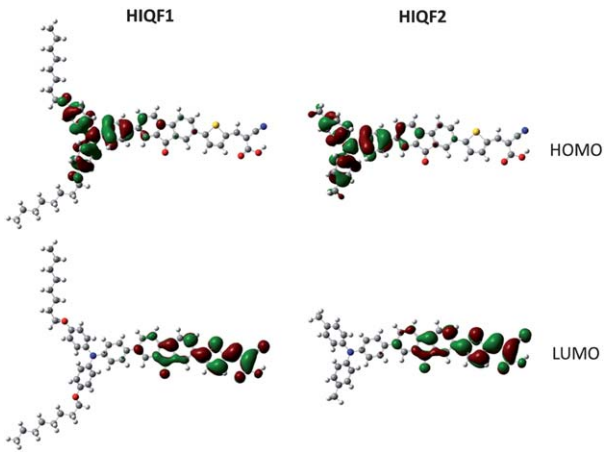

Fig. 4 Frontier molecular orbital profiles of **HIQF1** and **HIQF2** at the B3LYP/6-31G* level.

dithiophen-4-one was used as an additional acceptor in a D–A–A configuration for DSCs.[13] Because it was strongly electron withdrawing, the LUMO of this sensitizer dye was located predominantly on the 4*H*-cyclopenta[2,1-*b*:3,4-*b*']dithiophen-4-one moiety and then extended to the cyanoacetic acid units, resulting in low electron injection efficiency. Thus, the present results again demonstrate that fluorenone is a good candidate as an additional acceptor that not only effectively decreases the bandgap but also facilitates electron transport.

Device performances

The photovoltaic performance of DSCs sensitized by **HIQF1** and **HIQF2** was investigated under standard AM 1.5 irradiation (100 mW cm^{-2}) using an electrolyte composed of 0.6 M dimethylpropyl-imidazolium iodide, 0.05 M I_2, 0.1 M LiI, and 0.5 M *tert*-butyl pyridine in acetonitrile. Fig. 5 shows the photocurrent action spectra for DSCs sensitized with **HIQF1** and **HIQF2**, where the incident photon-to-current conversion efficiency (IPCE) values are plotted as a function of wavelength. Both dyes efficiently sensitized nanocrystalline TiO_2 over the whole visible range from 300 to 700 nm. **HIQF1** exhibited a slightly broader IPCE action spectrum than did **HIQF2**, and this result was attributed to the lower bandgap of HIQF1 owing to the presence of the alkoxy groups in its donor moiety. The IPCEs of the two dyes maintained a high plateau of about 80% throughout much of the visible region. Taking into account the reflection and absorption losses by the conducting glass of the DSCs, the efficiency of electric current generation in this range reached about 90% over a broad wavelength range extending from 350 to 600 nm. Thus, with further modification to increase the red-shift in absorbance, this type of novel fluorenone-based sensitizer dye could be very promising for high-efficiency DSCs.

Fig. 6 shows photocurrent–voltage (*J*–*V*) curves of DSCs sensitized with **HIQF1** and **HIQF2** under standard AM 1.5 solar light conditions. The short-circuit photocurrent density (J_{sc}), open-circuit voltage (V_{oc}), fill factor (FF) and overall conversion efficiency (η) for each dye-TiO_2 electrode are summarized in Table 2. The DSCs sensitized with **HIQF1** showed a J_{sc} of 12.26 mA cm^{-2}, a V_{oc} of 0.70 V, and a FF of 0.73, corresponding to an η value of 6.26%. Under the same device operating conditions, the current–voltage characteristics (J_{sc}, V_{oc}, FF, and η) of **HIQF2** were 11.46 mA cm^{-2}, 0.65 V, 0.76, and 5.66%, respectively. These results indicate that the attachment of long electron-donating alkoxy groups onto the donor unit of **HIQF1** slightly increased J_{sc}, V_{oc}, and η. These increases were attributed to the following reasons: (1) the electron-donating alkoxy groups – elevated the HOMO energy level and narrowed the bandgap of **HIQF1**, causing the dye to absorb longer-wavelength light and thus increasing J_{sc}; and (2) the introduction of the bulky alkoxy groups suppressed charge recombination between injected electrons and iodine, resulting in a higher V_{oc}. Thus, this class of alkoxy-substituted compounds serves as a basis for further design of new potential sensitizers fabricated by introducing suitable substituents on phenyl rings to enhance the light-harvesting efficiency of the sensitizer dye and, furthermore, to prevent surface aggregation of the sensitizer.[14]

CEM and IMVS characterization

To further understand the improvement in V_{oc} observed for DSCs sensitized with **HIQF1** and **HIQF2**, we first measured the relative conduction band position of TiO_2 by means of a charge extraction method developed by Frank *et al.*[15] As shown in Fig. 7.

DSCs sensitized with both **HIQF1** and **HIQF2** exhibited a linear increase in V_{oc} as a function of the logarithm of electron

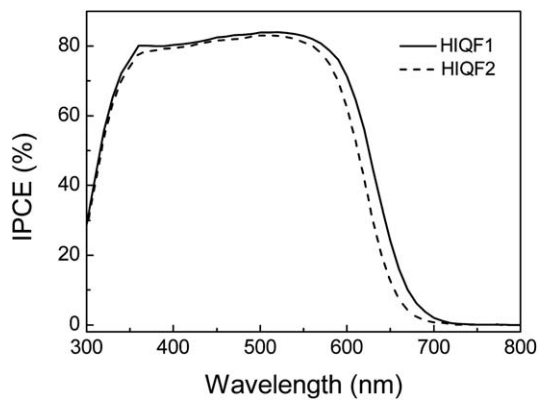

Fig. 5 IPCE spectra of DSCs based on **HIQF1** and **HIQF2**.

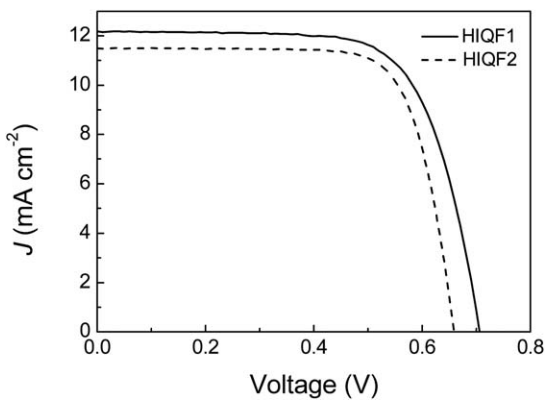

Fig. 6 *J*–*V* curves of DSCs sensitized with **HIQF1** and **HIQF2**.

Table 2 Current–voltage characteristics of DSCs sensitized with **HIQF1** and **HIQF2**

Dye	J_{sc} (mA cm^{-2})	V_{oc} [V]	FF	η (%)
HIQF1	12.26	0.70	0.73	6.26
HIQF2	11.46	0.65	0.76	5.66

density. Notably, the plots for the two dyes overlapped, indicating that DSCs sensitized with **HIQF1** or **HIQF2** had the same conduction band position regardless of the substituents on the triphenylamine donor unit. Since the conduction band edge was not influenced by these two dyes, the increase in V_{oc} for **HIQF1** compared to **HIQF2** should be ascribed to the suppression of charge recombination that is related to the electron lifetime (τ). Intensity-modulated photovoltage spectroscopy was used to measure τ, and Fig. 8 shows the relationship between τ and electron density for DSCs sensitized with **HIQF1** and **HIQF2**. **HIQF1** exhibited a much longer τ than **HIQF2** at the same electron density, implying that recombination between electrons on the TiO_2 surface and I_3^- ions in the electrolyte was considerably suppressed by **HIQF1** compared to **HIQF2**. Thus, the improvement in V_{oc} was attributed to suppression of charge recombination by the longer alkyl chains of **HIQF1**. Introduction of a stable fluorenone structure into the dye configuration can also be expected to improve DSC durability, and the stability of DSCs sensitized with these dyes is currently under investigation.

EIS characterization

We performed electrochemical impedance spectra to further study charge recombination kinetics at the TiO_2/dye/electrolyte interface under open circuit and illuminated conditions. As shown in Fig. 9, the Nyquist plots exhibited three semicircles, the largest semicircle (intermediate frequencies, 1–100 Hz) represents the electron transfer resistance (R_{CT}) at the TiO_2/dye/electrolyte interface, which showed R_{CT} in DSC based on **HIQF1** (5.44 Ω) is larger than that of **HIQF2** based cell (5.19 Ω), indicating that the electron recombination resistance increased from **HIQF2** to

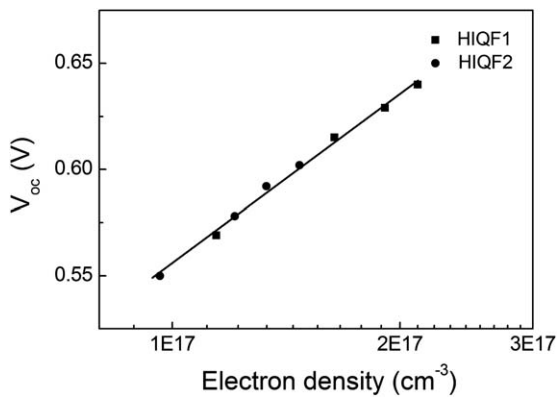

Fig. 7 V_{oc} as a function of electron density for DSCs sensitized with **HIQF1** and **HIQF2**. Electron density was measured by means of a charge extraction method.

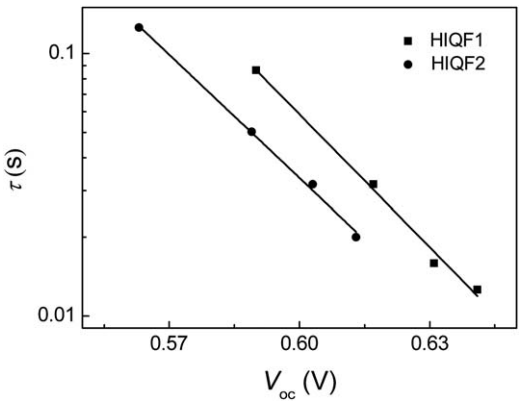

Fig. 8 Electron lifetime (τ) as a function of V_{oc} for DSCs sensitized with **HIQF1** and **HIQF2**. Electron lifetime was measured by means of intensity-modulated photovoltage spectroscopy.

HIQF1. The calculated electron lifetime increases from 7.8 ms (**HIQF2**) to 10.3 ms of **HIQF1**, which is derived from eqn (1):

$$\tau = C_{\mu} \times R_{CT} \quad (1)$$

where C_{μ} is interfacial chemical capacitance. This strongly supports the speculation that the bulky alkoxy groups of **HIQF1** can act as an effective blocker between the TiO_2 layer and the electrolyte, leading to more effective suppression of the back reaction of the injected electron with the I_3^- in the electrolyte, which is also reflected in the improved V_{oc}, yielding substantially enhanced DSCs efficiency.

In the Bode phase plot (as shown in Fig. 10), the middle-frequency peak (in the 1–100 Hz range) is indicative of the electron recombination between electrolyte and TiO_2. This parameter is related to the electron lifetime and is ultimately correlated with V_{oc}. The middle-frequency peaks of the DSCs based on **HIQF1** shift to lower frequency relative to that of **HIQF2**, indicating a longer recombination lifetime for the former case. This result is agreement with the fact that **HIQF1** possess higher V_{oc} values (0.70 V) than **HIQF2** (0.65 V). Thus, the presence of long alkyl chains in **HIQF1** increases not only charge generation and injection but also the electron lifetime, which leads to the both improvement of V_{oc} and J_{sc}, and ultimately the conversion efficiency.

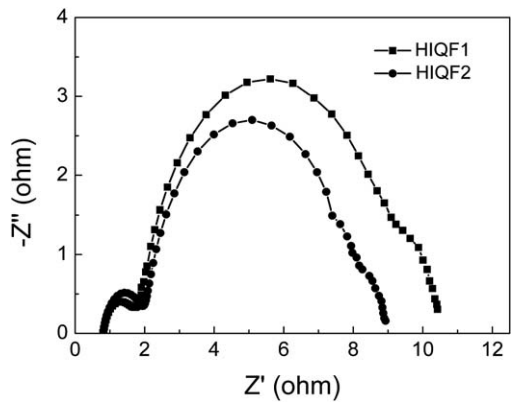

Fig. 9 EIS Nyquist plots for DSCs sensitized with **HIQF1** and **HIQF2**.

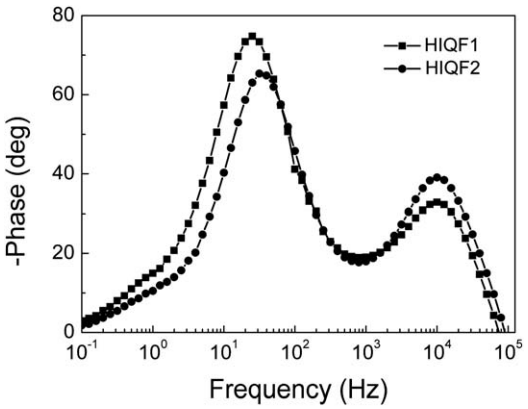

Fig. 10 EIS Bode plots for DSCs sensitized with **HIQF1** and **HIQF2**.

Conclusions

In summary, we have demonstrated for the first time the synthesis of two stable fluorenone-based sensitizer dyes, **HIQF1** and **HIQF2**, in which a fluorenone moiety served as an additional acceptor in a D–A–π–A framework. These dyes exhibited strong charge transfer absorption around 500 nm both in solution and adsorbed on TiO_2. Both dyes efficiently sensitized nanocrystalline TiO_2 over the whole visible range from 300 to 700 nm and maintained a high IPCE plateau of about 80% over most of the visible region. Addition of long alkoxy substituents in **HIQF1** not only slightly red-shifted the absorption spectrum but also suppressed charge recombination. As a result, solar cells sensitized with **HIQF1** showed a higher η (6.26%) compared to cells sensitized with **HIQF2** (5.66%). The results reported here provide preliminary evidence that fluorenone, which is both stable and inexpensive, is an effective building unit for high-efficiency DSC sensitizers. Further studies are underway to develop novel fluorenone-based sensitizer dyes for further broadening the absorption spectra to enhance the dyes' light-harvesting ability in the infrared wavelength region.

Experimental

Materials and instruments

Absorption spectra were measured in *N*,*N*-dimethylformamide (DMF) solution or on a TiO_2 film (thickness = 4 μm) with a UV-vis-NIR spectrophotometer (UV-3600, Shimadzu). ^{1}H (600 MHz) and ^{13}C NMR (150 MHz) spectra were measured with a DRX-600 spectrometer (Bruker BioSpin). Mass spectra were measured on a Shimadzu Biotech matrix-assisted laser desorption ionization (MALDI) mass spectrometer. Cyclic voltammetry was performed on a CH Instruments 624D potentiostat/galvanostat system. A conventional three-electrode configuration consisting of a platinum working electrode, a Pt-wire counter electrode, and an Ag/AgCl reference electrode was used. The solvent in all measurements was acetone nitrile, and the supporting electrolyte was 0.1 M $[Bu_4N]PF_6$. Ferrocene was added as a calibrant after each set of measurements, and all potentials reported were quoted with reference to the ferrocene-ferrocenium (Fc/Fc^+) couple at a scan rate of 50 mV s^{-1}. All chemicals and reagents were used as received from suppliers without further purification. THF and toluene were dried over molecular sieves and distilled under argon from sodium benzophenone ketyl immediately prior to use. 4-(4,4,5,5-tetramethyl-1,3,2-dioxaborolan-2-yl)-*N*,*N*-bis(4-ethyl-hexyloxyphenyl)-aniline and 4-(4,4,5,5-tetramethyl-1,3,2-dioxa-borolan-2-yl)-*N*,*N*-bis(4-methylphenyl)aniline were synthesized according the reference.[16] Column chromatography was performed using Wakogel-C300 as a stationary phase.

Dye synthesis and characterization

4-(7-Bromofluorenone-2-yl)-*N*,*N*-bis(4-ethylhexyloxyphenyl)-aniline. A mixture of 2,7-dibromofluorenone (0.34 g, 1 mmol), 4-(4,4,5,5-tetramethyl-1,3,2-dioxaborolan-2-yl)-*N*,*N*-bis(4-ethyl-hexyloxyphenyl)aniline and Pd $(PPh_3)_4$ (50 mg) were suspended in toluene (50 ml) and 2 M K_2CO_3 (10 ml) was refluxed for 24 h under argon. The crude product was extracted into dichloromethane, and the organic layer was washed with water and dried over anhydrous magnesium sulfate. After removal of the solvent under reduced pressure, the residue was purified by column chromatography on silica gel (hexane/dichloromethane, 1/2, v/v) to yield a yellow solid (0.68 g, 89.6%). ^{1}H NMR (600 MHz, $CDCl_3$, δ): 7.85 (s, 1H, Fn-H), 7.76 (d, J = 1.8 Hz, 1H, Fn-H), 7.68 (d, J = 7.2 Hz, 1H, Fn-H), 7.61 (dd, J = 7.8 Hz, J = 1.8 Hz, 1H, Fn-H), 7.52 (d, J = 7.8 Hz, 1H, Fn-H), 7.41 (m, 2H, Th-H), 7.39 (d, J = 7.8 Hz, 1H, Fn-H), 7.08 (s, 4H, Ph-H), 6.97 (s, 2H, Ph-H), 6.85 (d, J = 8.4 Hz, 4H, Ph-H), 3.82 (s, 4H, $-OCH_2-$), 1.72 (m, 2H, CH), 1.49 (m, 8H, $-CHCH_2CH_2-$), 1.32 (m, 8H, $-CH_2-$), 0.92 (m, 12H, $-CH_3$). ^{13}C NMR (150 MHz, $CDCl_3$, δ): 192.62, 156.03, 149.01, 143.17, 142.42, 141.42, 140.23, 137.18, 136.12, 138.48, 132.50, 130.72, 127.59, 127.16, 126.91, 122.53, 122.44, 121.60, 120.81, 119.99, 115.35, 70.74, 39.48, 30.56, 29.12, 23.88, 23.07, 14.11, 11.16. MS (MOLDI-TOF, m/z): $[M]^+$ calcd for $C_{47}H_{32}BrNO_3$. 757.3; found, 757.3.

5-{7-{4-[*N*,*N*-Bis(4-ethylhexyloxyphenyl)amino]phenyl}-fluorenone-2-yl}thiophenyl-2-carbaldehyde. The 5-formyl-2-thiopheneboronic acid (0.156 g, 1 mmol), 4-(7-bromofluorenone-2-yl)-*N*,*N*-bis(4-ethylhexyloxyphenyl)aniline (0.38 g, 0.5 mmol), $Pd(PPh_3)_4$ (10 mg) and K_2CO_3 (1 g), were dissolved in toluene (10 ml) and methanol (10 ml) and the solution was heated by microwave to reflux for 2 hours under the argon atmosphere. The crude product was extracted into dichloromethane, and the organic layer was washed with water and dried over anhydrous magnesium sulfate. After removal of the solvent under reduced pressure, the residue was purified by column chromatography on silica gel (hexane/dichloromethane, 1/2, v/v) to yield a red solid (0.3 g, 75%). ^{1}H NMR (600 MHz, $CDCl_3$, δ): 9.89 (s, 1H, CHO), 7.92 (s, 1H, Th-H), 7.86 (s, 1H, Th-H), 7.75 (m, 2H, Fn-H), 7.67 (m, 1H, Fn-H), 7.54 (d, J = 7.8 Hz, 2H, Fn-H), 7.45-7.41 (m, 3H, Ph-H + Fn-H), 7.09 (d, J = 8.4 Hz, 4H, Ph-H), 6.98 (d, J = 8.4 Hz, 2H, Ph-H), 6.86 (d, J = 8.4 Hz, 4H, Ph-H), 3.83 (m, 4H, $-OCH_2-$), 1.73 (m, 2H, –CH–), 1.44 (m, 8H, $-CHCH_2CH_2-$), 1.32 (m, 8H, $-CH_2-$), 0.94 (m, 12H, $-CH_3$). ^{13}C NMR (150 MHz, $CDCl_3$, δ): 193.18, 182.67, 156.06, 152.76, 149.06, 145.02, 142.68, 142.57, 141.45, 140.20, 137.34, 135.35, 135.11, 133.58, 132.47, 130.62, 127.19, 126.94, 124.47, 122.37, 121.85, 121.10, 120.88, 119.94, 115.37, 70.73, 39.48, 30.56, 29.13, 23.89, 23.08, 14.12,

11.17. MS (MOLDI-TOF, *m*/*z*): [M^+] calcd for $C_{52}H_{55}NO_4S$, 789.4; found, 789.5.

2-Cyano-3-{5-{7-{4-[*N*,*N*-bis(4-ethylhexyloxyphenyl)amino]-phenyl}-fluorenone-2-yl}thiophenyl}acrylic acid (HIQF1). To a stirred solution of 5-{7-{4-[*N*,*N*-bis(4-ethylhexyloxyphen-yl) amino]phenyl}-fluorenone-2-yl}thiophenyl-2-carbaldehyde (0.2 g, 0.25 mmol) and cyanoacetic acid (68 mg, 0.8 mmol) in chloroform (5 ml) was added piperidine (140 mg, 1.6 mmol). The reaction mixture was refluxed under argon for 12 h and then acidified with 2 M aqueous hydrochloric acid (10 ml). The crude product was extracted into chloroform, and the organic layer was washed with water and dried over anhydrous magnesium sulfate. After removal of the solvent under reduced pressure, the residue was purified by flash chromatography with chloroform and methanol/chloroform (1/10, v/v) in turn as eluents to yield a deep red powder (0.13 g, 79.2% yield). ^{1}H NMR (600 MHz, DMSO-d6, δ): 8.43 (s, 1H, C═CH), 8.01 (d, $J = 9$ Hz, 1H, Th-H), 7.98 (d, $J = 9$ Hz, 1H, Th-H), 7.95 (s, 1H, Fn-H), 7.92 (d, $J = 3.6$ Hz, 1H, Fn-H), 7.91 (d, $J = 7.8$ Hz, 1H, Fn-H), 7.86 (s, 2H, Fn-H), 7.82 (s, 1H, Fn-H), 7.61 (d, $J = 9$ Hz, 2H, Ph-H), 7.06 (d, $J = 8.4$ Hz, 4H, Ph-H), 6.94 (d, $J = 9$ Hz, 4H, Ph-H), 6.82 (d, $J = 9$ Hz, 2H, Ph-H), 3.84 (d, $J = 6$ Hz, 4H, –OCH_2–), 1.67 (m, 2H, –CH–), 1.43 (m, 8H, –$CHCH_2CH_2$–), 1.29 (m, 8H, –CH_2–), 0.88 (m, 12H, –CH_3). ^{13}C NMR (150 MHz, DMSO-d6, δ): 192.85, 163.76, 156.18, 149.06, 144.68, 141.86, 141.68, 140.85, 140.02, 135.78, 135.07, 134.95, 133.57, 133.22, 132.98, 130.03, 127.71, 127.58, 126.32, 122.68, 122.55, 121.55, 121.51, 119.28, 117.44, 116.03, 70.58, 39.20, 30.42, 28.93, 23.80, 23.00, 14.44, 11.42. HRMS (ESI, *m*/*z*): [M + H]$^+$ calcd for $C_{55}H_{56}N_2O_5S$, 856.3910; found, 856.3914. Anal. calcd for $C_{55}H_{56}N_2O_5S$: C 77.07, H 6.59, N 3.27; found: C 77.12, H 6.50, N 3.06%.

4-(7-Bromofluorenone-2-yl)-*N*,*N*-bis(4-methylphenyl)aniline. 4-(4,4,5,5-tetramethyl-1,3,2-dioxaborolan-2-yl)-*N*,*N*-bis(4-methylphenyl)aniline (0.4 g, 1 mmol), 2,7-dibromofluorenone (0.34 g, 1 mmol) and Pd (PPh_3)$_4$ (50 mg) were suspended in toluene (50 ml) and 2 M K_2CO_3 (10 ml), and the resulting mixture was heated to reflux for 16 hours under the argon atmosphere. After completion of the reaction, water (120 ml) was added to the reaction solution, and this was extracted with dichloromethane, dried with magnesium sulfate, and concentrated under reduced pressure. The residue was purified by silica gel column chromatography (hexane/dichloromethane = 1/2) to obtain 4-(7-bromofluorenone-2-yl)-*N*,*N*-bis(4-methylphenyl)aniline as a red solid (0.36 g, 68%). ^{1}H NMR (600 MHz, $CDCl_3$, δ): 7.86 (d, $J =$ 1.8 Hz, 1H, Fn-H), 7.77 (d, $J = 1.8$ Hz, 1H, Fn-H), 7.69 (dd, $J =$ 7.8 Hz, $J = 1.8$ Hz, 1H, Fn-H), 7.61 (dd, $J = 7.8$ Hz, $J = 1.8$ Hz, 1H, Fn-H), 7.53 (d, $J = 7.8$ Hz, 1H, Fn-H), 7.45 (d, $J = 7.2$ Hz, 2H, Ph-H), 7.41 (d, $J = 7.8$ Hz, 1H, Fn-H), 7.10 (d, $J = 8.4$ Hz, 4H, Ph-H), 7.07 (s, 1H, Ph-H), 7.06 (s, 1H, Ph-H), 7.04 (d, $J = 8.4$ Hz, 4H, Ph-H), 2.33 (s, 6H, –CH_3). ^{13}C NMR (150 MHz, $CDCl_3$, δ): 192.56, 148.39, 144.94, 143.11, 142.29, 141.63, 137.20, 136.11, 134.48, 133.06, 132.66, 132.01, 130.02, 127.61, 127.27, 125.00, 122.61, 122.56, 122.11, 121.64, 120.83, 20.88. MS (MOLDI-TOF, *m*/*z*): [M^+] calcd for $C_{33}H_{24}BrNO$. 529.1; found, 529.5.

5-{7-{4-[*N*,*N*-Bis(4-methylphenyl)amino]phenyl}-fluorenone-2-yl}thiophenyl-2-carbaldehyde. The 5-formyl-2-thiopheneboronic acid (0.156 g, 1 mmol), 4-(7-bromofluorenone-2-yl)-*N*,*N*-bis(4-methylphenyl)aniline (0.27 g, 0.5 mmol) and Pd(PPh_3)$_4$ (10 mg) were dissolved in toluene (30 ml) and 2 M K_2CO_3 (5 ml), and the solution was heated to reflux for 24 hours under the argon atmosphere. To the reaction solution was added water (50 ml), and this was extracted with dichloromethane, dried with magnesium sulfate, and concentrated under reduced pressure. The residue was purified by silica gel column chromatography (hexane/dichloromethane = 1/2) to obtain 5-{7-{4-[*N*,*N*-bis-(4-methylphenyl)amino]phenyl}-fluore-none-2-yl}thiophenyl-2-carbaldehyde (0.48 g, 85%). ^{1}H NMR (600 MHz, $CDCl_3$, δ): 9.91 (s, 1H, CHO), 7.96 (d, $J = 1.8$ Hz, 1H, Th-H), 7.91 (d, $J = 1.8$ Hz, 1H, Th-H), 7.80 (dd, $J = 7.8$ Hz, $J = 1.8$ Hz, 1H, Fn-H), 7.77 (d, $J = 3.6$ Hz, 1H, Fn-H), 7.73 (dd, $J = 7.8$ Hz, $J = 1.8$ Hz, 1H, Fn-H), 7.59 (d, $J = 7.8$ Hz, $J = 1.8$ Hz, 2H, Fn-H), 7.45 (m, 3H, Ph-H), 7.09 (m, 5H, Ph-H), 7.07 (s, 1H, Ph-H), 7.05 (d, $J = 8.4$ Hz, 4H, Ph-H), 2.33 (s, 6H). ^{13}C NMR (150 MHz, DMSO-d6, δ): 193.19, 182.73, 152.77, 148.45, 144.99, 142.72, 142.48, 141.70, 139.11, 137.39, 135.38, 135.13, 133.69, 133.10, 132.69, 132.54, 131.94, 130.03, 127.30, 125.03, 124.52, 122.55, 122.08, 121.93, 121.14, 120.96, 20.88. MS (MOLDI-TOF, *m*/*z*): [M^+] calcd for $C_{38}H_{27}NO_2S$, 561.2; found, 561.4.

2-Cyano-3-{5-{7-{4-[*N*,*N*-bis(4-methylphenyl)amino]phenyl}-fluorenone-2yl}thiophenyl}-acrylic acid (HIQF2). HIQF2 was synthesized according to the procedure described for HIQF1 and was obtained as a deep red powder (0.15 g, 75% yield). ^{1}H NMR (600 MHz, DMSO-d6, δ): 8.37 (s, 1H, COOH), 8.32 (s, 1H, C═CH), 8.01 (d, $J = 7.8$ Hz, 1H, Th-H), 7.95 (d, $J = 7.8$ Hz, 1H, Th-H), 7.93 (s, 1H, Fn-H), 7.89 (m, 4H, Fn-H), 7.85 (s, 1H, Fn-H), 7.66 (d, $J = 8.4$ Hz, 2H, Ph-H), 7.16 (d, $J = 8.4$ Hz, 4H, Ph-H), 6.98 (d, $J = 8.4$ Hz, 4H, Ph-H), 6.95 (d, $J = 8.4$ Hz, 2H, Ph-H), 2.26 (s, 6H, –CH_3). ^{13}C NMR (150 MHz, DMSO-d6, δ): 192.84, 163.66, 148.31, 144.84, 144.50, 141.97, 141.66, 136.11, 135.09, 134.96, 133.75, 133.35, 133.19, 131.49, 130.66, 127.85, 126.26, 125.35, 122.70, 122.61, 121.72, 121.69, 121.48, 20.91. HRMS (ESI, *m*/*z*): [M + H]$^+$ calcd for $C_{41}H_{28}N_2O_3S$, 628.1821; found, 628.1823. Anal. calcd for $C_{41}H_{28}N_2O_3S$: C 78.32, H 4.49, N 4.46; found: C 78.36, H 4.26, N 4.43%.

Cell fabrication and characterization

The DSCs were fabricated as follows. A double-layer TiO_2 photoelectrode (thickness 15 μm; area 0.25 cm^2) was used as a working electrode. A 10 μm main transparent layer with titania particles (~20 nm) and a 5 μm scattering layer with titania particles (~400 nm) were screen-printed on the fluorine-doped tin oxide conducting glass substrate. A solution of **HIQF1** and **HIQF2** (3×10^{-4} M) in acetonitrile/*tert*-butyl alcohol (1/1, v/v) was used to coat the TiO_2 film with the dye. Deoxycholic acid (20 mM) was added to the dye solution as a co-adsorbent to prevent aggregation of the dye molecules. The electrodes were immersed in the dye solutions and then kept at 25 °C for 24 h to adsorb the dye onto the TiO_2 surface. The dye-coated TiO_2 film was used as the working electrode, and platinum-coated conducting glass was used as the counter-electrode. The two electrodes were separated by a Surlyn spacer (50 μm thick) and sealed up by heating the polymer frame. The electrolyte was composed of 0.6 M dimethylpropylimidazolium iodide, 0.05 M

I_2, 0.1 M LiI and 0.5 M *tert*-butyl pyridine in acetonitrile. The current–voltage characteristics were measured using a black metal mask and edge with an aperture area of 0.25 cm^2 under standard AM 1.5 sunlight (100 mW cm^{-2}, WXS-155S-10: Wacom Denso Co. Japan).[17] Monochromatic incident photon-to-current conversion efficiency spectra were measured with monochromatic incident light of 1×10^{16} photons cm^{-2} under 100 mW cm^{-2} in director current mode (CEP-2000BX, Bunko-Keiki).

Acknowledgements

This work was supported by NIMS Saint-Gobain Center of Excellence for Advanced Materials and Core Research for Evolutional Science and Technology (CREST) of the Japan Science and Technology Agency.

References

1 (*a*) B. O'Regan and M. Grätzel, *Nature*, 1991, **353**, 737; (*b*) A. Yellla, H.-W. Lee, H. Tsao, C. Yi, A. K. Chandiran, M. K. Nazeerudin, E. W.-G. Diau, C.-Y. Yeh, S. M. Zakeeruddin and M. Grätzel, *Science*, 2011, **334**, 629; (*c*) T. Horiuchi, H. Miura, K. Sumioka and S. Uchida, *J. Am. Chem. Soc.*, 2004, **126**, 12218; (*d*) M. Zhang, Y. Cao, Y. Bai, Y. Wang, Y. Shi, M. Zhang, F. Wang, C. Pan and P. Wang, *Chem. Mater.*, 2010, **22**, 1915.

2 (*a*) A. Hagfeldt, G. Boschloo, L. C. Sun, L. Kloo and H. Pettersson, *Chem. Rev.*, 2010, **110**, 6595; (*b*) Z. Ning, Y. Fu and H. Tian, *Energy Environ. Sci.*, 2010, **3**, 1170; (*c*) F. Gao, Y. Wang, D. Shi, J. Zhang, M. Wang, X. Jing, R. Humphry-Baker, P. Wang, S. M. Zakeeruddin and M. Grätzel, *J. Am. Chem. Soc.*, 2008, **130**, 10720; (*d*) H. J. Snaith, A. J. Moule, C. Klein, K. Meerholz, R. H. Friend and M. Grätzel, *Nano Lett.*, 2007, **7**, 3372; (*e*) C. Qin, W. Peng, K. Zhang, A. Islam and L. Han, *Org. Lett.*, 2012, **14**, 2532.

3 (*a*) M. Velusamy, K. R. J. Thomos, J. Lin, Y. Hsu and K.-C. Ho, *Org. Lett.*, 2005, **7**, 1899; (*b*) W. Zhu, Y. Wu, S. Wang, W. Li, X. Li, J. Chen, Z.-S. Wang and H. Tian, *Adv. Funct. Mater.*, 2011, **21**, 756; (*c*) D. W. Chang, H. J. Lee, J. H. Kim, S. Y. Park, S.-M. Park, L. Dai and J.-B. Baek, *Org. Lett.*, 2011, **13**, 3880; (*d*) Y. Cui, Y. Wu, X. Lu, X. Zhang, G. Zhou, F. B. Miapeh, W. Zhu and Z.-S. Wang, *Chem. Mater.*, 2011, **23**, 4394.

4 (*a*) M. Gross, D. C. Müller, H.-G. Nothofer, U. Scherf, D. Neher, C. Bräuchle and K. Meerholz, *Nature*, 2000, **405**, 661; (*b*) U. Scherf and E. J. W. List, *Adv. Mater.*, 2002, **14**, 477; (*c*) Q. Zheng, S. Gupta, G. He, L. Tan and P. Prasad, *Adv. Funct. Mater.*, 2008, **18**, 2770.

5 W. Li, Y. Wu, X. Li, Y. Xie and W. Zhu, *Energy Environ. Sci.*, 2011, **4**, 1830.

6 H. Hogel, G. Barchietto and D. Tar, *Photochem. Photobiol.*, 2008, **16**, 335.

7 (*a*) E. Zojer, A. Pogantsch, E. Hennebicq, D. Beljonne, J.-L. Brédas, P. Scandiucci de Freitas, U. Scherf and E. J. W. List, *J. Chem. Phys.*, 2002, **117**, 6794; (*b*) L. Oldridge, M. Kastler and K. Müllen, *Chem. Commun.*, 2006, 885.

8 L. A. Estrada, J. E. Yarnell and D. C. Neckers, *J. Phys. Chem. A*, 2011, **115**, 6366.

9 K.-F. Chen, Y.-C. Hsu, Q.-Y. Wu, M.-C. P. Yeh and S.-S. Sun, *Org. Lett.*, 2009, **11**, 377.

10 G. Oskam, B. V. Bergeron, G. J. Meyer and P. C. Searson, *J. Phys. Chem. B*, 2001, **105**, 6867.

11 M. K. Nazeeruddin and M. Grätzel, in *Encyclopedia of Electronchemistry: Semiconductor Electrodes and Photoelectronchemistry*, ed. A. Bard, M. Startmann and S. Licht, Wiley-VCH, Germany, 2002, pp. 407–431.

12 A. Hagfeld and M. Grätzel, *Chem. Rev.*, 1995, **95**, 49.

13 C. Qin, A. Islam and L. Han, *Dyes Pigm.*, 2012, **94**, 553.

14 (*a*) M. Zhang, Y. Cao, Y. Bai, Y. Wang, Y. Shi, M. Zhang, F. Wang, C. Pan and P. Wang, *Chem. Mater.*, 2010, **22**, 1915; (*b*) Q.-Y. Yu, J.-Y. Liao, S.-M. Zhou, Y. Shen, J.-M. Liu, D.-B. kuang and C.-Y. Su, *J. Phys. Chem. C*, 2011, **115**, 22002.

15 G. Schlichthoerl, S. Y. Huang, J. Sprague and A. J. Frank, *J. Phys. Chem. B*, 1997, **101**, 8141.

16 L. Chen, B. Zhang, Y. Cheng, Z. Xie, L. Wang, X. Jing and F. Wang, *Adv. Funct. Mater.*, 2010, **20**, 3143.

17 (*a*) N. Koide and L. Han, *Rev. Sci. Instrum.*, 2004, **75**, 2828; (*b*) N. Koide, Y. Chiba and L. Han, *Jpn. J. Appl. Phys.*, 2005, **44**, 4176.